Preparation of $Zn_{(1-x)}Cd_xFe_2O_4$ (x = 0.0, 0.1, 0.3, 0.5, 0.7 and 1.0) ferrite samples and their characterization by Mössbauer and positron annihilation techniques

2007 J. Phys.: Condens. Matter 19 236210

(http://iopscience.iop.org/0953-8984/19/23/236210)

IOP PUBLISHING JOURNAL OF PHYSICS: CONDENSED MATTER

J. Phys.: Condens. Matter **19** (2007) 236210 (11pp) doi:10.1088/0953-8984/19/23/236210

Preparation of $Zn_{(1-x)}Cd_xFe_2O_4$ ($x = 0.0$, 0.1, 0.3, 0.5, 0.7 and 1.0) ferrite samples and their characterization by Mössbauer and positron annihilation techniques

Mahuya Chakrabarti[1], **D Sanyal and A Chakrabarti**

Variable Energy Cyclotron Centre, 1/AF, Bidhannagar, Kolkata 700064, India

E-mail: mahuasanyal2003@rediffmail.com

Received 7 February 2007, in final form 18 April 2007
Published 11 May 2007
Online at stacks.iop.org/JPhysCM/19/236210

Abstract

Single phase $Zn_{(1-x)}Cd_xFe_2O_4$ ($x = 0.0$, 0.1, 0.3, 0.5, 0.7 and 1.0) ferrite samples have been prepared by the solid state reaction method. The room temperature Mössbauer spectra for all the samples indicate the paramagnetic nature of the prepared samples. Mössbauer spectra have been deconvoluted separately for the tetrahedral 'A' site and the octahedral 'B' site to identify the variations of the Mössbauer parameters, i.e. isomer shift, quadrupole splitting and linewidth, with the concentration of Cd doping, x, for the tetrahedral 'A' site and octahedral 'B' site. Changes of these parameters with concentration, x, confirm that the Cd^{2+} ions prefer to go to the tetrahedral 'A' site compared to the octahedral 'B' site in this $Zn_{(1-x)}Cd_xFe_2O_4$ cubic spinel ferrite system. To study the changes in the electron momentum distributions, coincidence Doppler broadening of the electron positron annihilation γ-radiation measurement technique has been employed. The results indicate that positrons are annihilating less with the oxygen 2p electrons and other core electrons in the case of mixed ($Zn_{(1-x)}Cd_xFe_2O_4$) ferrites than $ZnFe_2O_4$ or $CdFe_2O_4$ ferrites.

(Some figures in this article are in colour only in the electronic version)

1. Introduction

Since the recent past ferrites either in the microcrystalline phase or in the nanocrystalline phase have drawn a lot of attention due to their unique magnetic as well as electrical properties [1]. Among them the spinel ferrites, MFe_2O_4, where M = Co, Ni, Mg, Zn, Cd etc, have many applications, e.g., in microwave devices, gas sensors, information storage systems etc. [2, 3]. In the spinel structured materials there are two sites, tetrahedral A sites and octahedral B

[1] Author to whom any correspondence should be addressed.

sites. In the normal spinel structured materials, e.g. $ZnFe_2O_4$, $CdFe_2O_4$ etc, tetrahedral A sites are occupied by the Zn^{2+} and Cd^{2+} ions whereas the octahedral B sites are occupied by the Fe^{3+} ions [4]. Both $ZnFe_2O_4$ and $CdFe_2O_4$ are normal spinels in which the $ZnFe_2O_4$ shows antiferromagnetic behaviour below 10.5 K whereas for $CdFe_2O_4$ it is below 12 K [5, 6]. The spinel ferrites can be prepared by different methods, e.g. the solid-state reaction method [7], the sol–gel method [8], the wet chemical method [9] etc.

In the present work, $Zn_{(1-x)}Cd_xFe_2O_4$ ($x = 0.0$, 0.1, 0.3, 0.5, 0.7 and 1.0) ferrite samples have been prepared by the solid state reaction method. The sintering temperature and time have been optimized by ensuring the single phase of the prepared samples. The single phase of the prepared samples, its average particle size and lattice parameter a have been determined by the powder x-ray diffraction method. The local magnetic properties of the prepared samples have been studied by employing the ^{57}Fe (14.4 keV) Mössbauer technique [4].

The variations of the electron momentum distributions due to systematic doping of Cd in the $Zn_{(1-x)}Cd_xFe_2O_4$ system have been studied by employing the coincidence Doppler broadening of the electron positron annihilation γ-radiation (CDBEPAR) measurement technique [10, 11]. In the CDBEPAR spectroscopic technique a positron from the radioactive (^{22}Na) source is thermalized inside the material under study and annihilated with an electron, emitting two oppositely directed 511 keV γ-rays [10]. Depending upon the momentum of the electron (p) these 511 keV γ-rays are Doppler shifted by an amount $\pm\Delta E$ in the laboratory frame, where

$$\Delta E = p_L c/2$$

p_L is the component of the electron momentum, p, along the detector direction. By using a high resolution HPGe detector one can measure the Doppler shifts of these 511 keV γ-rays. The wing part of the 511 keV photo-peak carries the information about the annihilation of positrons with the higher momentum electrons, e.g. core electrons of different atoms. Using two HPGe detectors in coincidence and placed at an angle 180° with respect to each other, it is possible to reduce the background in the 511 keV photo-peak drastically [11]. This allows the study of positron annihilation with the higher momentum electrons with a much better precision. Thus by measuring the Doppler broadening of the 511 keV γ-rays and proper analysis of the CDBEPAR spectrum [11] one can identify the electrons with which the positrons are annihilating.

2. Experimental outline

Ferrite ($Zn_{(1-x)}Cd_xFe_2O_4$ with $x = 0.0$, 0.1, 0.3, 0.5, 0.7 and 1.0) samples have been prepared by the standard solid state reaction method from a stoichiometric mixture of α-Fe_2O_3 (purity 99.998%, Alfa Aesar, Johnson Matthey, Germany), ZnO (purity 99.998%, Alfa Aesar, Johnson Matthey, Germany) and CdO (purity 99.998%, Alfa Aesar, Johnson Matthey, Germany). The mixture is first ball milled in a Fritsch Pulverisette 5 planetary ball mill grinder with agate balls for 1 h and then calcined at different temperatures in air, followed by slow cooling. The different calcination temperatures for different samples have been listed in table 1. The sintering temperature is kept the same as the calcination temperature. The resulting material is then pressed (∼220 MPa pelletizing pressure) in the form of pellets. The cubic spinel structure of the materials has been confirmed by the x-ray diffraction pattern (figure 1). The x-ray diffraction data are collected on a Philips 1710 automatic diffractometer with Cu K_α radiation. For each sample a scan has been performed from 4° to 90° with a step size of 0.02°. The average particle size of the sample has been calculated from the Williamson–Hall plot [12] i.e.

$$\beta \cos\theta = K\lambda/D + 2\varepsilon \sin\theta$$

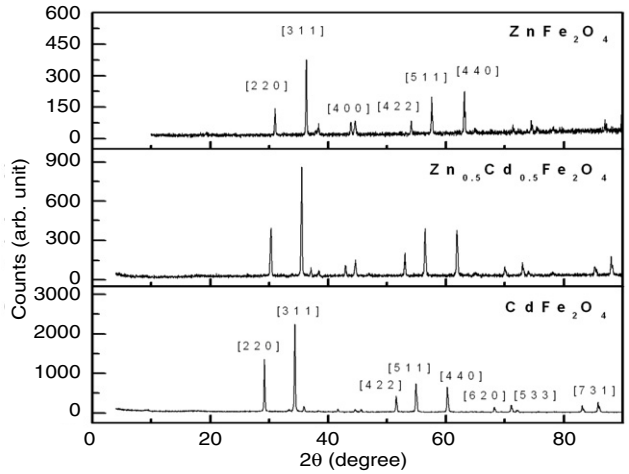

Figure 1. X-ray diffraction (XRD) pattern of the $ZnFe_2O_4$, $Zn_{0.5}Cd_{0.5}Fe_2O_4$ and $CdFe_2O_4$ samples.

Table 1. The calcination temperature, T, and the time duration, H, for the preparation of $Zn_{(1-x)}Cd_xFe_2O_4$ ($x = 0.0$, 0.1, 0.3, 0.5, 0.7 and 1.0) samples.

x	T (°C)	H (h)
0.0	1100	3
0.1	1050	3
0.3	1050	3
0.5	970	3
0.7	950	3
1.0	900	3

where D is the average particle size, β is the FWHM, K is a constant (=0.89), λ is the wavelength, θ is the Bragg angle and ε is the strain introduced inside the sample.

Room temperature ^{57}Fe Mössbauer spectra for all the samples have been recorded in the transmission configuration with constant acceleration mode. A gas filled proportional counter has been used for the detection of 14.4 keV Mössbauer γ-rays, while a 10 mCi ^{57}Co isotope embedded in an Rh matrix has been used as the Mössbauer source. The Mössbauer spectrometer has been calibrated with 95.16% enriched $^{57}Fe_2O_3$ and standard α-^{57}Fe foil. The Mössbauer spectra have been analysed by a standard least square fitting program (NMOSFIT).

For the CDBEPAR measurement, two identical HPGe detectors (efficiency, 12%; type, PGC 1216sp from DSG, Germany), having energy resolution of 1.1 keV at 514 keV of ^{85}Sr, have been used as two 511 keV γ-ray detectors, while the CDBEPAR spectra have been recorded in a dual ADC-based multiparameter data acquisition system (MPA-3 from FAST ComTec., Germany). An about 10 μCi ^{22}Na positron source (enclosed in between thin Mylar foils) has been sandwiched between two identical and plane faced pellets [13]. The peak to background ratio of this CDBEPAR measurement system, with $\pm\Delta E$ selection, is $\sim 10^5$:1.

3. Results and discussion

Table 1 represents the calcination temperature and corresponding duration for the preparation of different samples. It is clear from table 1 that for lower concentration higher calcination

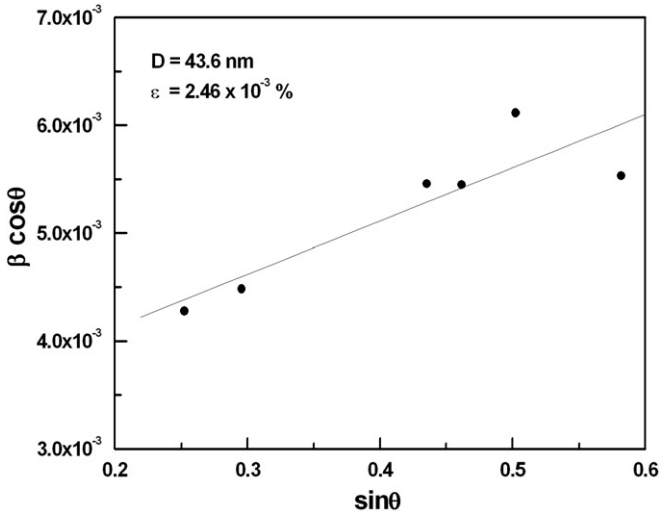

Figure 2. Williamson–Hall plot of the $CdFe_2O_4$ sample.

Table 2. Average particle size, D, and the strain in $Zn_{(1-x)}Cd_xFe_2O_4$ ($x = 0.0$, 0.1, 0.3, 0.5, 0.7 and 1.0) samples.

x	D (nm)	Strain (%)
0.0	35	4.40×10^{-4}
0.1	44	1.62×10^{-3}
0.3	58	3.50×10^{-3}
0.5	33	2.28×10^{-3}
0.7	39	2.15×10^{-3}
1.0	44	2.46×10^{-3}

temperature is required. Li *et al* [14] prepared the $ZnFe_2O_4$ samples by the solid state reaction method with the calcination temperature of 1200 °C for a duration of 48 h. In the present case the same preparation process with a ball mill grinding and mixing method (∼1 h) before calcination has been adopted. This reduces the duration of the calcination process (∼3 h). Thus the method is very useful to prepare ferrite samples within a very short time. In the case of $CdFe_2O_4$ samples the reported calcination temperature is 900 °C and the duration is 12 h [7], but for the present case the samples have been calcined at 900 °C for 3 h only. The sintering temperature is kept the same as the calcination temperature.

Figure 1 shows the x-ray diffraction (XRD) pattern for the $ZnFe_2O_4$, $Zn_{0.5}Cd_{0.5}Fe_2O_4$ and $CdFe_2O_4$ samples. The XRD peaks confirm the cubic spinel structure for all the samples. The average particle size and the strain introduced inside the samples have been calculated by the Williamson–Hall plot [12]. A typical Williamson–Hall plot for the $CdFe_2O_4$ sample has been shown in figure 2. Average particle sizes and strains have been calculated from the slope and the intercept of the fitted straight line, respectively. The average particle size and the strain introduced inside the sample for all the samples obtained from the Williamson–Hall plot are listed in table 2. It is clear from table 2 that the doping does not greatly affect the average particle size of the ferrite samples but the doping concentration strongly increases the strain introduced inside the samples. The lattice parameters a for all the cubic spinel structured samples have been calculated from different diffraction lines of the XRD pattern (figure 1).

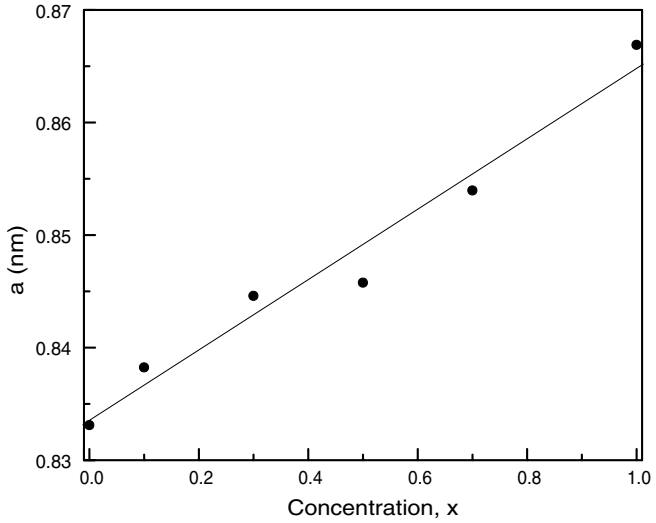

Figure 3. Variation of the lattice parameter, a, with Cd^{2+} concentration, x, in the $Zn_{(1-x)}Cd_xFe_2O_4$ system.

Figure 3 shows the variation of the lattice parameter a with Cd^{2+} concentration, x. It is seen from figure 3, that the lattice parameter increases linearly with concentration, x. The lattice parameters a for $ZnFe_2O_4$ and $CdFe_2O_4$ samples have been calculated as 0.833 and 0.867 nm, respectively, which are very close to the literature value (0.844 and 0.869 nm for $ZnFe_2O_4$ and $CdFe_2O_4$ samples, respectively) [15]. The larger value of lattice parameter a for $CdFe_2O_4$ compared to $ZnFe_2O_4$ is due to the larger ionic radius of Cd^{2+} than Zn^{2+}.

The radii of the tetrahedral (R_{tetra}) and octahedral (R_{octa}) sites, the tetrahedral (R_{Ax}) and octahedral (R_{Bx}) bond length, the tetrahedral edge length (R_{xx}), the shared octahedral edge length ($R_{x'x}$) and the unshared octahedral edge length ($R_{x''x}$) of these cubic mixed spinel oxides have been calculated by using the following equations [16]:

$$
\begin{aligned}
R_{\text{tetra}} &= \sqrt{3}(u - 1/4)a - R_0 \\
R_{\text{octa}} &= \{3u^2 - (11/4)u + 43/64\}^{1/2}a - R_0 \\
R_{Ax} &= \sqrt{3}(u - 1/4)a \\
R_{Bx} &= \{3u^2 - (11/4)u + 43/64\}^{1/2}a \\
R_{xx} &= \sqrt{2}(2u - 1/2)a \\
R_{x'x} &= \sqrt{2}(1 - 2u)a \\
R_{x''x} &= \{4u^2 - 3u + 11/16\}^{1/2}a
\end{aligned}
$$

where u is the oxygen parameter ($u = 0.385$, 0.3859, 0.38705, 0.38827, 0.3895 and 0.3911 for $Zn_{(1-x)}Cd_xFe_2O_4$ samples with $x = 0.0$, 0.1, 0.3, 0.5, 0.7 and 1.0 respectively [16]), and a is the lattice parameter. $R_0 = 1.38$ Å [17] is the radius of the oxygen atom. These values are summarized in table 3. Figure 4 shows the variations of the radii of the tetrahedral sites and the octahedral sites with Cd^{2+} concentration, x, in the $Zn_{(1-x)}Cd_xFe_2O_4$ system. From figure 4 it is clear that R_{tetra} increases linearly with x but R_{octa} remains almost constant. From table 3 it is clear that the tetrahedral bond length also increases sharply with x, whereas the octahedral bond length remains almost constant. This is because the larger ionic radius Cd^{2+}

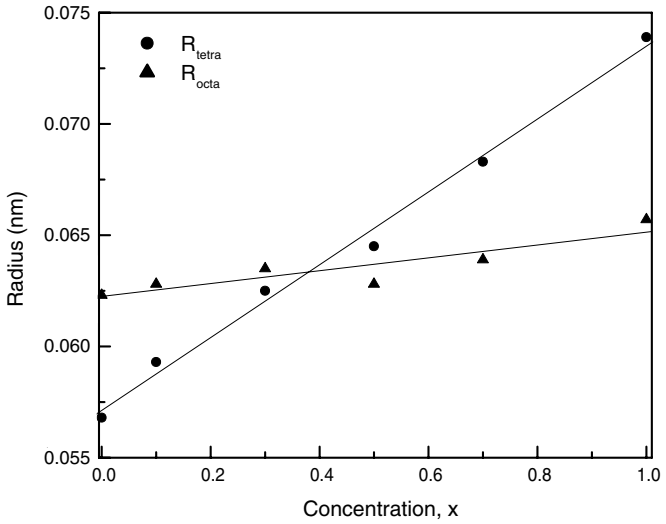

Figure 4. Variations of the radii of the tetrahedral sites and the octahedral sites with Cd^{2+} concentration, x.

Table 3. Values of tetrahedral and octahedral bond length and tetrahedral, shared octahedral and unshared octahedral edge length for the $Zn_{(1-x)}Cd_xFe_2O_4$ ($x = 0.0$, 0.1, 0.3, 0.5, 0.7 and 1.0) samples.

Concentration of Cd, x	Tetrahedral bond length (pm)	Octahedral bond length (pm)	Tetrahedral edge length (pm)	Shared octahedral edge length (pm)	Unshared octahedral edge length (pm)
0.0	195	200	318	271	295
0.1	197	201	322	271	297
0.3	201	202	327	270	299
0.5	202	201	331	267	300
0.7	206	202	337	267	303
1.0	212	201	346	267	308

is replacing the smaller ionic radius Zn^{2+} in the tetrahedral sites in the $Zn_{(1-x)}Cd_xFe_2O_4$ cubic spinel ferrites.

Figures 5(a) and (b) represent the room temperature Mössbauer spectra for the $Zn_{(1-x)}Cd_xFe_2O_4$ ($x = 0.0$, 0.1, 0.3, 0.5, 0.7 and 1.0) samples. It is clear from these figures that all the samples show a doublet type of Mössbauer spectra and no ferromagnetic nature (six line pattern of Mössbauer spectra) has been observed. Some spectral broadening is also observed, which increases with increasing concentration of Cd^{2+} in the $Zn_{(1-x)}Cd_xFe_2O_4$ system. This spectral broadening is due to the changes in the tetrahedral bond length and due to the change in the Zn^{2+}, Cd^{2+} and Fe^{3+} ionic distributions in the tetrahedral and octahedral sites of this $Zn_{(1-x)}Cd_xFe_2O_4$ cubic spinel ferrite system. From the experimental Mössbauer spectra both isomer shift (IS) and quadrupole splitting (QS) have been calculated by a standard least square fitting program, NMOSFIT. Figure 6 represents the variation of the isomer shift and the quadrupole splitting with the concentration, x, of Cd^{2+} in the $Zn_{(1-x)}Cd_xFe_2O_4$ system. The typical values of IS and QS for the $ZnFe_2O_4$ sample are 0.115 and 0.335 mm s^{-1}, respectively. The variations of the Mössbauer parameters (IS and QS) with the concentration, x, of Cd in the $Zn_{(1-x)}Cd_xFe_2O_4$ system have been depicted in figure 6.

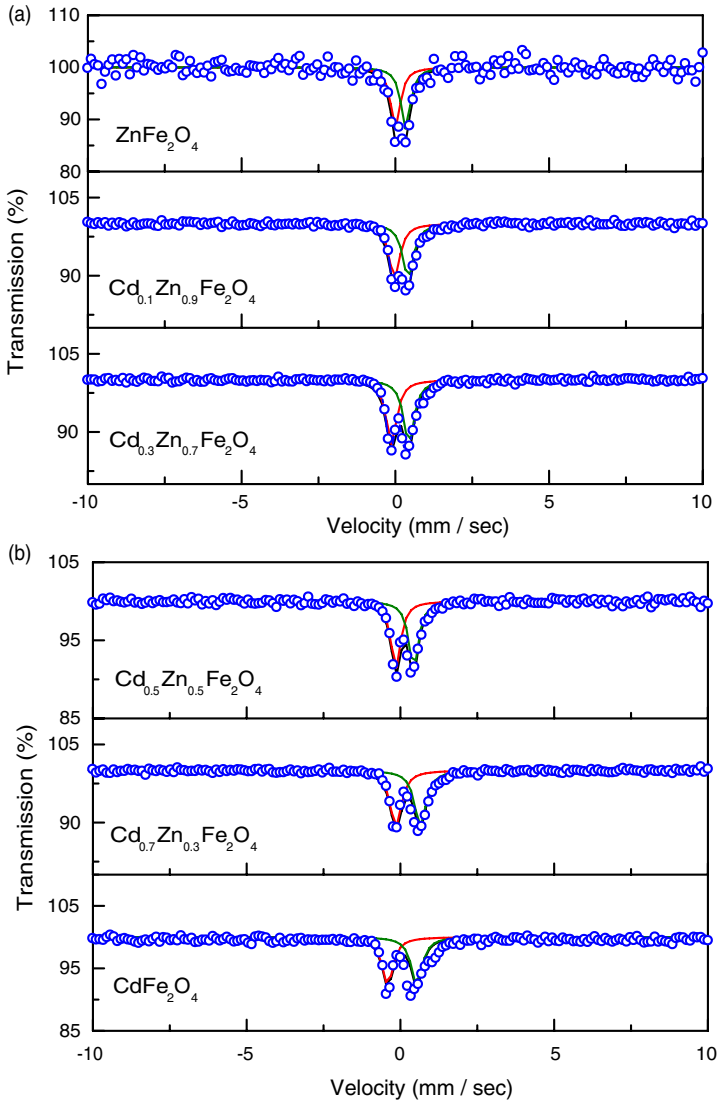

Figure 5. (a) Room temperature Mössbauer spectra for the $Zn_{(1-x)}Cd_xFe_2O_4$ ($x = 0.0$, 0.1 and 0.3) samples. (b) Room temperature Mössbauer spectra for the $Zn_{(1-x)}Cd_xFe_2O_4$ ($x = 0.5$, 0.7 and 1.0) samples.

The isomer shift and the linewidth value have also been deconvoluted separately for the tetrahedral 'A' site and the octahedral 'B' site of this spinel system due to doping of the Cd^{2+} ion. Figure 7 represents the variation of the isomer shift and the linewidth for the 'A' site and 'B' site of this $Zn_{(1-x)}Cd_xFe_2O_4$ cubic spinel ferrite system with Cd^{2+} concentration, x. From this figure it is clear that the isomer shift for the tetrahedral 'A' site increases, whereas for the octahedral 'B' site it decreases, which suggests that the s electron density at the 'B' site decreases and for the 'A' site it increases due to the substitution of Cd^{2+} in the $Zn_{(1-x)}Cd_xFe_2O_4$ system. The linewidth also increases for the tetrahedral 'A' site compared to the octahedral 'B' site. Thus, due to incorporation of the larger ionic radius Cd^{2+} ion in place of the Zn^{2+} ion

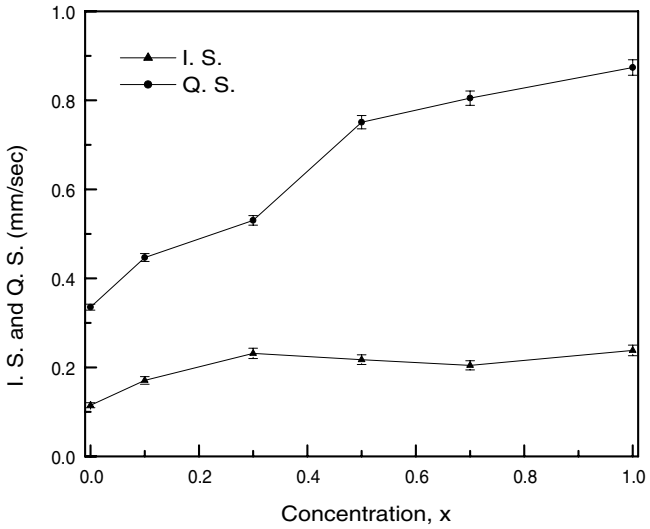

Figure 6. Variation of the isomer shift (IS) and the quadrupole splitting (QS) with Cd^{2+} concentration, x.

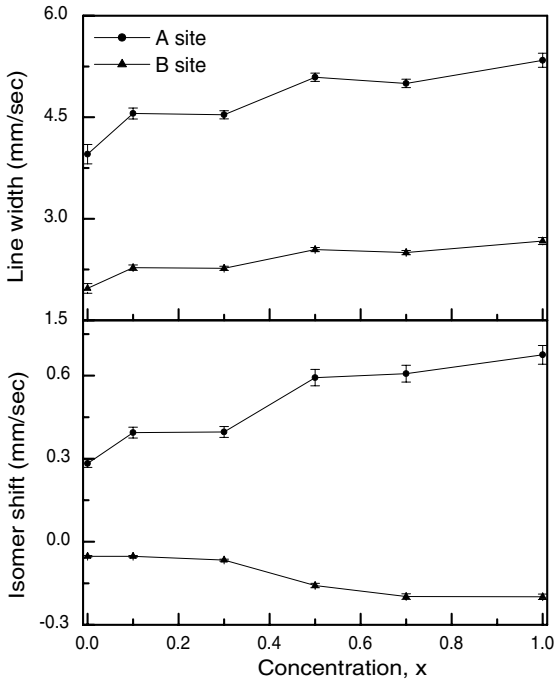

Figure 7. Variation of the isomer shift and the linewidth for the tetrahedral 'A' site and octahedral 'B' site of the $Zn_{(1-x)}Cd_xFe_2O_4$ cubic spinel ferrite system with Cd^{2+} concentration, x.

in the tetrahedral 'A' site of the $Zn_{(1-x)}Cd_xFe_2O_4$ cubic spinel ferrite system, both Mössbauer parameters increase.

Doping of Cd^{2+} in the $Zn_{(1-x)}Cd_xFe_2O_4$ cubic spinel ferrite system may introduce some defects inside the samples. To study this effect the coincidence Doppler broadening of the

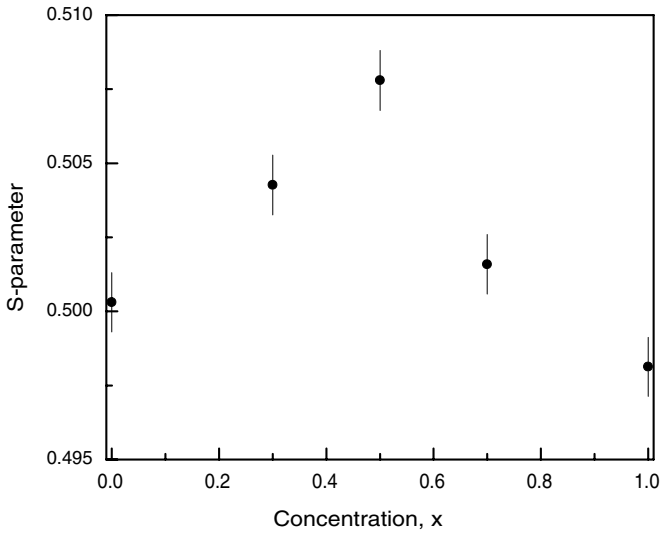

Figure 8. Variation of S-parameter with Cd^{2+} concentration, x, in the $Zn_{(1-x)}Cd_xFe_2O_4$ cubic spinel ferrite.

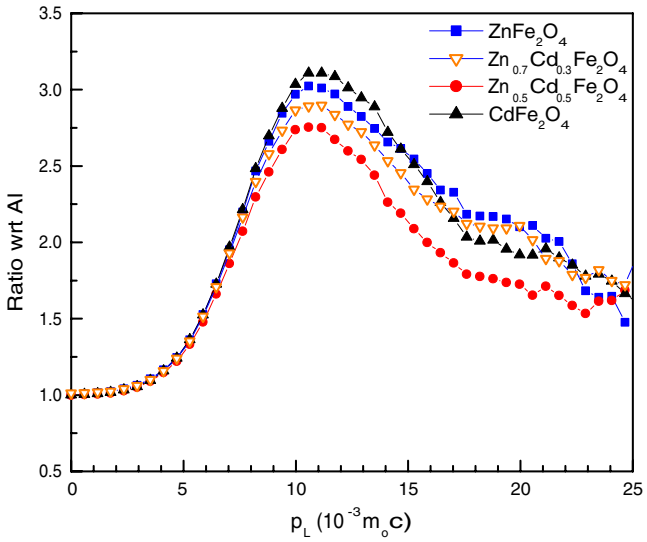

Figure 9. Ratios of the experimental electron positron momentum distributions for $ZnFe_2O_4$, $Zn_{0.7}Cd_{0.3}Fe_2O_4$, $Zn_{0.5}Cd_{0.5}Fe_2O_4$ and $CdFe_2O_4$ systems to the electron–positron momentum distributions of a 99.9999% pure defect free Al single crystal.

electron positron annihilation γ-radiation spectrum has been analysed by evaluating the so called line-shape parameter (S-parameter) [18]. The S-parameter is calculated as the ratio of the counts in the central area of the 511 keV photo-peak ($|511\ \text{keV} - E_\gamma| \leqslant 0.85$ keV) and the total area of the photo-peak ($|511\ \text{keV} - E_\gamma| \leqslant 4.25$ keV). The S-parameter represents the fraction of positrons annihilating with the lower momentum electrons with respect to the total electrons annihilated. Figure 8 represents the variation of S parameter with Cd^{2+} concentration, x. From this figure it is observed that the value of S parameter is almost the same for both

$ZnFe_2O_4$ and $CdFe_2O_4$ while the S-parameter has an increased value for mixed ferrite systems, i.e. $Zn_{(1-x)}Cd_xFe_2O_4$, $x = 0.3, 0.5, 0.7$. This suggests that in the case of mixed ferrite systems either positrons are annihilating more with the lower momentum electrons or annihilating less with the higher momentum electrons such as core electrons of different atomic sites. For better understanding, CDBEPAR spectra have been analysed by constructing the ratio curve [19, 20] with respect to the CDBEPAR spectrum of a defect free Al (99.9999% pure) single crystal. Figure 9 represents the ratio curves for the $ZnFe_2O_4$, $Zn_{0.7}Cd_{0.3}Fe_2O_4$, $Zn_{0.5}Cd_{0.5}Fe_2O_4$ and $CdFe_2O_4$ systems. Generally, the ratio curve for oxide materials with respect to Al shows a peak at $\sim 11 \times 10^{-3} m_0 c$, which is primarily due to the annihilation of positrons with oxygen 2p electrons [20, 21]. From figure 9 it is clear that the annihilation of positrons with the oxygen 2p electrons and other core electrons decreases in the case of mixed ferrites ($Zn_{(1-x)}Cd_xFe_2O_4$, $x = 0.3, 0.5, 0.7$) compared with the $ZnFe_2O_4$ and $CdFe_2O_4$ systems. This suggests formation of more oxygen defects in the mixed ferrite system. Thus the reason behind the increased value of S-parameter, in the case of the mixed ferrite system, is less annihilation of positrons with the oxygen 2p electrons and with other core electrons in this system.

4. Conclusion

$Zn_{(1-x)}Cd_xFe_2O_4$ ($0 \leqslant x \leqslant 1$) ferrites have been prepared by the solid state reaction method with ball mill grinding and mixing processes. The lattice parameter and the tetrahedral and octahedral site radii have been calculated by analysing the XRD pattern. The room temperature Mössbauer spectra for all the prepared samples indicate the paramagnetic nature of the prepared samples at room temperature. Isomer shift, quadrupole splitting and linewidth have been calculated separately for the tetrahedral 'A' site and the octahedral 'B' site for all the prepared samples by deconvoluting the room temperature Mössbauer spectra. Changes of these parameters with concentration x confirm that in this $Zn_{(1-x)}Cd_xFe_2O_4$ cubic spinel ferrite system Cd^{2+} ions prefer to go to the tetrahedral 'A' site compared to the octahedral 'B' site. To observe the changes in the electron momentum distributions in these $Zn_{(1-x)}Cd_xFe_2O_4$ ($0 \leqslant x \leqslant 1$) spinel ferrites, coincidence Doppler broadening of the electron positron annihilation radiation measurement technique has been employed. From the results of CDBEPAR measurement it has been concluded that the positrons are less annihilating with the oxygen 2p electrons in the mixed ferrites ($Zn_{(1-x)}Cd_xFe_2O_4$, $x = 0.3, 0.5$ and 0.7) than the $ZnFe_2O_4$ and $CdFe_2O_4$ systems.

Acknowledgment

M Chakrabarti gratefully acknowledges the Council of Scientific and Industrial Research, Government of India, for providing financial assistance.

References

[1] Yokoyama M, Ohta E, Sato T and Sato T 1998 *J. Magn. Magn. Mater.* **183** 173
Roy M K, Halder Bidyut and Verma H C 2006 *Nanotechnology* **17** 232
[2] Kittel C 1996 *Introduction to Solid State Physics* 7th edn (New York: Wiley)
[3] Xiangfeng C, Xingqin L and Guangyao M 2000 *Sensors Actuators* **65** 64
[4] Greenwood N N and Gibb T C 1971 *Mössbauer Spectroscopy* (London: Chapman and Hall)
[5] Goya G F and Rechenberg H R 1999 *J. Magn. Magn. Mater.* **196/197** 191
[6] Mostafa A A, EI-Shobaky G A and Girgis E 2006 *J. Phys. D: Appl. Phys.* **39** 2007
[7] Mahmouda M H, Abdallasa A M, Hamdehb H H, Hikalb W M, Taherb S M and Hob J C 2003 *J. Magn. Magn. Mater.* **263** 269

[8] Lee J-G, Park J Y, Oh Y-J and Kim C S 1998 *J. Appl. Phys.* **84** 2801
[9] Petrera M, Gennaro A and Burriesci N 1982 *J. Mater. Sci.* **17** 429
[10] Hautojärvi P and Corbel C 1995 *Positron Spectroscopy of Solids* ed A Dupasquier and A P Mills Jr (Amsterdam: IOS Press) p 491
[11] Lynn K G and Goland A N 1976 *Solid State Commun.* **18** 1549
[12] Williamson G K and Hall W H 1953 *Acta Metall.* **1** 22
[13] Sanyal D, Banerjee D and De U 1998 *Phys. Rev.* B **58** 15226
Chakrabarti M, Dutta S, Chattapadhyay S, Sarkar A, Sanyal D and Chakrabarti A 2004 *Nanotechnology* **15** 1792
[14] Li F S, Wang L, Wang J B, Zhou Q G, Zhou X Z, Kunkel H P and Willams G 2004 *J. Magn. Magn. Mater.* **268** 332
[15] JCPDS-ICDD, PCPDFWIN 1.1, 1995 22-1010 22-1063
[16] Otero Arean C, Garcia Diaz E, Rubio Gonzalez J M and Villa Garcia M A 1988 *J. Solid State Chem.* **77** 275
[17] Shannon R D 1976 *Acta Crystallogr.* A **32** 751
[18] Chakrabarti M, Sarkar A, Chattapadhyay S, Sanyal D, Bhattacharya R and Banerjee D 2003 *Solid State Commun.* **128** 321
[19] Ghosh V J, Alatalo M, Asoka-Kumar P, Nielsen B, Lynn K G, Kruseman A C and Mijnarends P E 2000 *Phys. Rev.* B **61** 10092
[20] Chakrabarti M, Sarkar A, Sanyal D, Karwasz G P and Zecca A 2004 *Phys. Lett.* A **321** 376
[21] Myler U and Simpson P J 1997 *Phys. Rev.* B **56** 14303